Maximizing Ag Utilization in High-Rate CO_2 Electrochemical Reduction with a Coordination Polymer-Mediated Gas Diffusion Electrode

Wang, Riming; Haspel, Henrik; Pustovarenko, Alexey; Dikhtiarenko, Alla; Osadchii, Dmitrii; Ma, Ming; Smith, Wilson A.; Kapteijn, Freek; Gascon, Jorge

DOI
10.1021/acsenergylett.9b01509

Publication date
2019

Document Version
Final published version

Published in
ACS Energy Letters

ACS Energy LETTERS

Cite This: ACS Energy Lett. 2019, 4, 2024−2031

http://pubs.acs.org/journal/aelccp

LETTER

Maximizing Ag Utilization in High-Rate CO_2 Electrochemical Reduction with a Coordination Polymer-Mediated Gas Diffusion Electrode

Riming Wang,[†] Henrik Haspel,[‡] Alexey Pustovarenko,[‡] Alla Dikhtiarenko,[‡] Artem Russkikh,[‡] Genrikh Shterk,[‡] Dmitrii Osadchii,[†] Samy Ould-Chikh,[‡] Ming Ma,[§] Wilson A. Smith,[§] Kazuhiro Takanabe,[‡,∥] Freek Kapteijn,[†] and Jorge Gascon*[,‡]

[†]Catalysis Engineering, Dept. of Chemical Engineering, Faculty of Applied Sciences, Delft University of Technology, van der Maasweg 9, 2629 HZ Delft, The Netherlands

[‡]King Abdullah University of Science and Technology, KAUST Catalysis Center, Advanced Catalytic Materials, Thuwal 23955, Saudi Arabia

[§]Materials for Energy Conversion and Storage (MECS), Dept. of Chemical Engineering, Faculty of Applied Sciences, Delft University of Technology, Van der Maasweg 9, 2629 HZ Delft, The Netherlands

[∥]Department of Chemical Systems Engineering, School of Engineering, The University of Tokyo, 7-3-1 Hongo, Bunkyo-ku 113-8656, Japan

Supporting Information

ABSTRACT: We report the preparation and electrocatalytic performance of silver-containing gas diffusion electrodes (GDEs) derived from a silver coordination polymer (Ag-CP). Layer-by-layer growth of the Ag-CP onto porous supports was applied to control Ag loading. Subsequent electro-decomposition of the Ag-CP resulted in highly selective and efficient CO_2-to-CO GDEs in aqueous CO_2 electroreduction. Afterward, the metal−organic framework (MOF)-mediated approach was transferred to a gas-fed flow electrolyzer for high current density tests. The in situ formed GDE, with a low silver loading of 0.2 mg cm^{-2}, showed a peak performance of $j_{CO} \approx 385$ mA cm^{-2} at around −1.0 V vs RHE and stable operation with high FE_{CO} (>96%) at $j_{Total} = 300$ mA cm^{-2} over a 4 h run. These results demonstrate that the MOF-mediated approach offers a facile route for manufacturing uniformly dispersed Ag catalysts for CO_2 electrochemical reduction by eliminating ill-defined deposition steps (drop-casting, etc.) while allowing control of the catalyst structure through self-assembly.

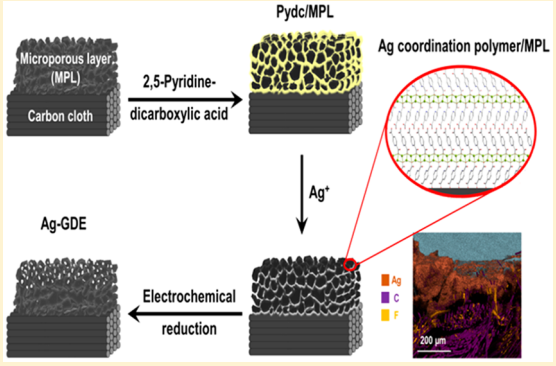

Atmospheric CO_2 concentration has been increasing drastically since the industrial revolution; this has spurred different initiatives into reducing emissions and directly utilizing CO_2.[1−5] Among the various methods proposed, CO_2 electrochemical reduction (CO_2ER) is one of the most promising technologies because of the relatively mild operating conditions and the increasing sources of green electricity.[6−8] Moreover, the electrochemical reduction of CO_2 can be driven toward one single product, avoiding expensive purification and separation steps. In this sense, the selective electrochemical conversion of CO_2 to CO constitutes an excellent perspective technology. Au,[9,10] Ag,[11,12] and Zn[13] have been identified as the most efficient catalysts for this process. The high price of Au and the low stability of Zn place Ag as the most attractive option.[12,14−19] As is the case in classical heterogeneous catalysis, optimization of the final catalyst composition and metal loading are critical to the commercialization of CO_2ER. Most studies to date have focused on the application of metal plates[12,20] or supported nanoparticles.[9−11,13,21] In the former case, the high metal content per electrode area results in such high capital expenditures (CAPEX) that these technologies become nonviable. There-

Received: July 15, 2019
Accepted: July 29, 2019
Published: July 29, 2019

DOI: 10.1021/acsenergylett.9b01509
ACS Energy Lett. 2019, 4, 2024−2031

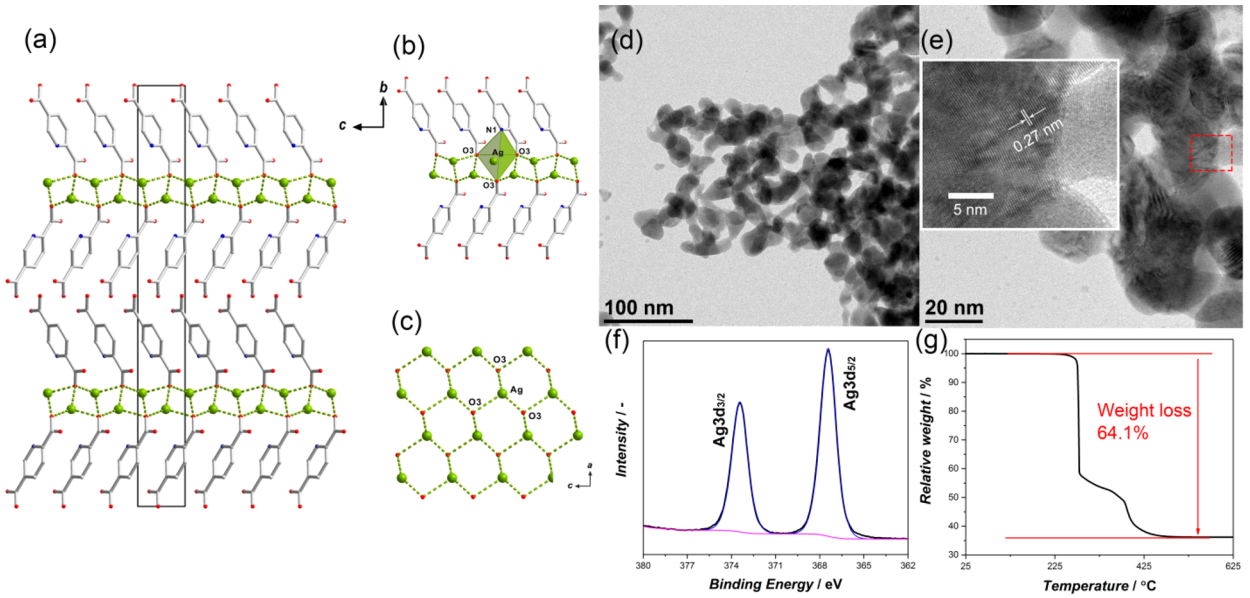

Figure 1. (a) Representation of the lamellar crystal packing and the unit cell of Ag-CP viewed along the *a*-axis. (b) Coordination mode of 2,5-pyridinedicarboxylic acid (μ_3-bridging through O3 atom). (c) Hexagonal arrangement of Ag in the polymeric layer. Color scheme of the atoms: silver, green; carbon, gray; oxygen, red; nitrogen, blue. Hydrogen atoms are omitted for clarity. (d) Low- and (e) high-magnification TEM images of Ag-CP. The inset in panel e is a magnified image of the red box area. (f) XPS Ag 3d regional spectrum of Ag-CP and (g) TGA curve of Ag-CP in air.

fore, the use of supported metal catalysts seems more realistic. Catalyst layer morphology has an effect on cathode performance: a more uniform active phase distribution and lower particle agglomeration lead to better catalytic performance.[22] However, the fabrication of uniformly dispersed catalysts remains a significant challenge. Herein, we propose the metal−organic framework (MOF)-mediated synthesis as a facile and scalable method for manufacturing highly dispersed supported Ag catalysts with very low metal loadings for CO_2ER.

The use of metal−organic frameworks as catalyst precursors has gained significant attention in the past few years.[23−27] Following this approach, a presynthesized MOF is treated at high temperature in a controlled atmosphere and transformed into a supported metal nanoparticle catalyst.[28] The high activities per metal atom exhibited by the resulting catalysts, even when the total metal content can be as high as 50 wt %,[23] demonstrate the enormous potential of this approach. In this work, we demonstrate that MOF-mediated synthesis (MOFMS) can also be realized through electro-decomposition.

Here, a Ag coordination polymer (Ag-CP) is grown directly onto carbon-based microporous layer (MPL) gas diffusion electrodes by a layer-by-layer (LBL) method, followed by the electro-decomposition of the coordination polymer to achieve a well-defined carbon-supported Ag structure (denoted as Ag/MPL). The in situ formed carbon cloth supported Ag gas diffusion electrodes exhibit high CO_2ER efficiency in both the traditional aqueous three-electrode system and a gas-fed flow electrolyzer. Overcoming CO_2 transport limitations in the latter resulted in a peak performance of j_{CO} = 385 mA cm^{-2} CO partial current density and 1864 mA mg^{-1} mass activity due to the extremely low Ag loading. The work opens up the possibility for the direct manufacture of CO_2ER electrodes with optimum catalyst utilization using the MOF-mediated approach.

The self-assembly between 2,5-pyridinedicarboxylic (pydc) acid and $AgNO_3$ in several common solvents at room temperature leads to the formation of a Ag-CP microcrystalline powder (Tables S1 and S2 and Figure S1).[29] The crystal structure of Ag-CP was elucidated from powder X-ray diffraction (PXRD) data by means of simulated annealing procedure followed by Rietveld refinement.[30−32] The Ag-CP crystallizes in the orthorhombic $Pbn2_1$ space group (Figures S2 and S3 and Table S3) and reveals a layered arrangement of silver atoms coordinated to 2,5-pydc ligands (Figure S4 and Table S4). The linker moieties lie on both sides of the Ag ion double layer: one carboxylic group is bonded to three crystallographically equivalent silver atoms exhibiting a μ_3-bridging mode; another one is protonated and participates in the formation of hydrogen bonds between two Ag-CP 2D networks (Figures 1a−c and S5).

Characterization results of Ag-CP are displayed in Figure 1d−g. The Ag-CP particles have a particle size ranging from 25 to 35 nm (Figure 1d). The high-magnification TEM image (inset of Figure 1e) shows well-defined *d*-spacing with a distance of ∼0.27 nm. The Ag 3d XPS spectrum of Ag-CP (Figure 1f) exhibits two highly symmetric peaks with binding energies of 367.4 and 373.4 eV, corresponding to Ag $3d_{5/2}$ and Ag $3d_{3/2}$ photoelectron lines, respectively. The photoelectron shift of the Ag 3d line reveals that only oxidized Ag is present in the sample, which agrees with the Ag−O interaction in the crystal structure. The survey XPS spectrum of Ag-CP (Figure S6) proves the presence of Ag, C, N, and O in the sample, and the atomic content of each element is summarized in Table S5. The TGA curve of Ag-CP (Figure 1g) exhibits a total weight loss of ∼64.1%. Because Ag_2O is thermodynamically unfavorable at high temperatures,[33] the final product is metallic Ag with a silver content of ∼35.9%. The formation of metallic Ag after the high-temperature calcination of Ag-CP in air can also be confirmed by XRD (Figure S7). N_2

DOI: 10.1021/acsenergylett.9b01509
ACS Energy Lett. 2019, 4, 2024−2031

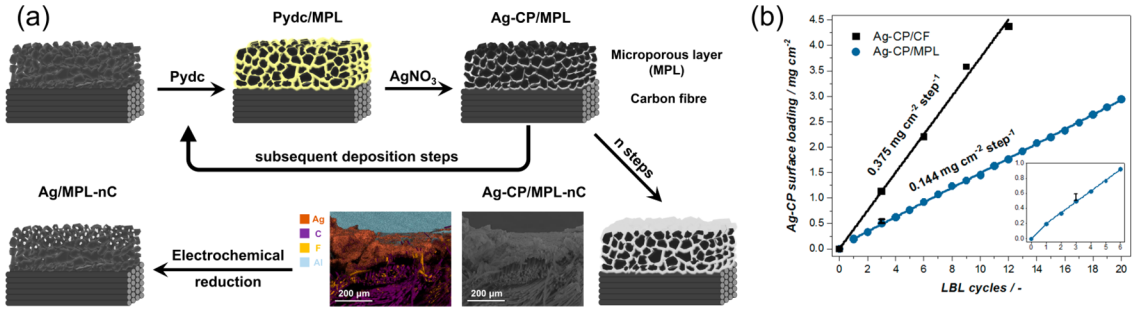

Figure 2. Scheme of the preparation of Ag/MPL catalysts, sequential deposition of Ag-CP via alternating adsorption of the dicarboxylic linker and the metal node, and cross-sectional elemental maps of C, F, Ag, and Al (a). Fluorine can be found on the PTFE-treated carbon fabric, while the Al signal comes from the sample holder. Surface loading as a function of deposition steps on bare carbon fiber and MPL/carbon cloth (b). The error bar at the 3 LBL point was determined from 8 different samples.

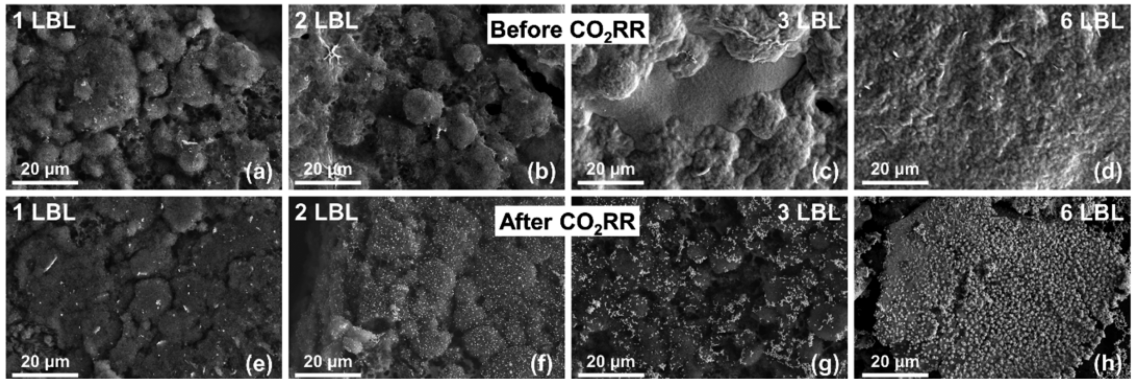

Figure 3. SEM images of electrodes prepared with 1 (a and e), 2 (b and f), 3 (c and g), and 6 (d and h) LBL cycles before and after electro-decomposition.

physisorption of Ag-CP (Figure S8) shows a type II isotherm and absence of microporosity.

Ag-CP was deposited onto the support by the subsequent adsorption of pydc and Ag^+ from their DMF solutions (Figure 2a). The Ag-CP loading increases strictly linearly from the second deposition step (LBL cycle) up to 12 or 20 cycles, as is seen in Figure 2b for bare carbon fiber and MPL containing carbon cloth alike. Utilizing the top part of the microporous layer, however, helps to achieve good surface coverage at lower Ag-CP loading (0.144 ↔ 0.375 mg cm^{-2} $step^{-1}$). Taking the theoretical density of the unit cell (2.557 g cm^{-3}) from Table S3 into consideration, a 0.563 μm thick Ag-CP layer (and because the longest cell parameter is around 3.2 nm, practically) of 150−200 unit cell thickness is deposited in each cycle onto the MPL support. The higher-than-linear deposition in the first LBL cycle (Figure 2b, inset) is due to the high surface area of the carbon grains in the MPL, as first the Ag-CP is built up directly onto the carbon surface (see EDS elemental maps of a 20 LBL sample in Figures 2a and S9). The actual CO_2ER catalyst is then formed by the in situ electrochemical reduction of the supported coordination polymer (Figure 2a). The final Ag loading also changes linearly with the number of deposition steps, as is seen in the bare carbon fiber-based samples (Ag/CF-*n*C, *n* = 3, 6, 9, 12) in Figure S10. The difference between the Ag-CP and Ag loading was ∼35.2 wt %, which is in good agreement with the Ag content in the crystallographically determined formula (39.4 wt %) and with the previous TGA analysis (∼35.9 wt %).

Although several MOF-derived electrocatalysts have been reported in the literature recently, to the best of our knowledge, no detailed mechanistic description of the electrochemical reduction and transformation of MOFs into the resulting NPs exists. We propose that as the reducing potential is applied to the electrode and the metal node is reduced back to zero valence silver, the linker molecules are not able to coordinate, and hence maintain, the continuous polymeric structure anymore. The collapsing structure releases silver atoms at the surface of the support, and nanoparticles and—with increasing Ag-CP coverage—the agglomerated silver network are formed through conventional aggregation.

According to the SEM images (Figures 3 and S11−S14), Ag-CP fully covers the MPL of the gas diffusion electrode after at least 2 LBL cycles (Figure 3a−d). A spot of Ag-CP on the 1 LBL sample is clearly seen in Figure S11a, whereas in Figures S12a−14a the CP coverage is continuous. The subsequent electro-decomposition of Ag-CP resulted in well-dispersed Ag nanoparticles (Figure 3e−h) due to the homogeneous distribution of the Ag-CP precursor. The Ag/MPL-1C electrode (Figure 3e) has a relatively sparse distribution of Ag particles, while Ag/MPL-6C shows an agglomerated network of silver structures. Well-dispersed individual Ag particles were obtained by using 2 and 3 LBL cycles (Figure 3f,g). Although the thick carbon fabric-supported Ag NPs are not suitable for TEM investigation, we removed the MPL grains by ultrasonication, and the Ag particle size distributions were determined (Figure S15). Because no significant differences in the PSDs were found, we propose that there is no direct connection between variation of activity and particle size in our system.

DOI: 10.1021/acsenergylett.9b01509
ACS Energy Lett. 2019, 4, 2024−2031

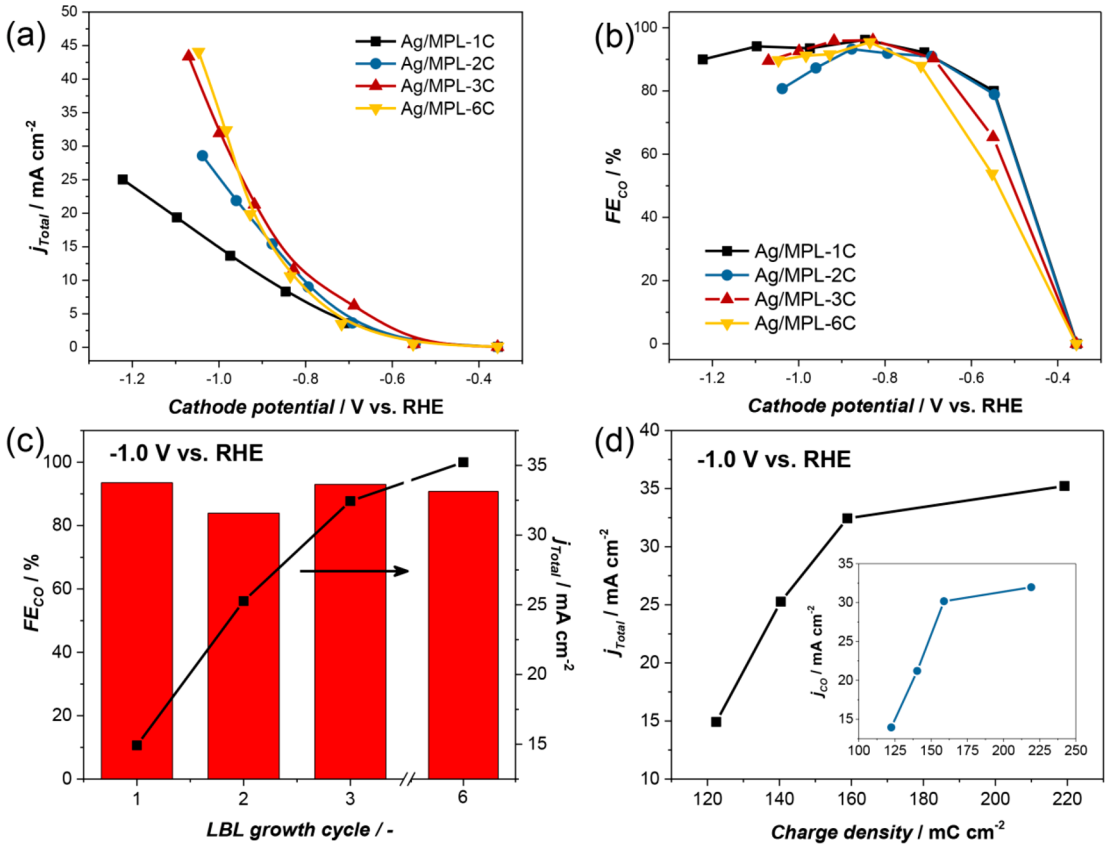

Figure 4. CO_2 electrochemical reduction performance of Ag/MPL-*n*C electrodes. (a) Total current density, (b) FE for CO, and (c) their LBL cycle dependency at −1.0 V vs RHE. (d) Variation of j_{Total} and j_{CO} with the electrochemical active surface area (EASA) at the same potential.

After the LBL growth process, the PXRD pattern of the carbon cloth-supported Ag-CP is compared with the simulated pattern of the pure Ag-CP in Figure S16a. The sharp reflections demonstrate the good crystallinity of Ag-CP. The position of the Ag-CP/CF reflections corresponds well to those of the simulated material. After the electro-decomposition process, metallic Ag is formed (Figure S16b), with three major reflections centered at 44.6°, 52.5°, and 77.2° corresponding to the (111), (200), and (220) crystal facets of metallic Ag. The broad peak centered at ∼27° is likely to be generated by the amorphous carbon in the carbon support. After CO_2ER, the metallic Ag pattern is maintained, demonstrating the stability of the electrode.

Evolution of Ag chemical states in the sample before and after in situ catalyst formation (i.e., in CO_2 electrolysis) were determined by XPS (Figure S17). After deconvolution, two doublets can be distinguished in the Ag 3d line, corresponding to metallic Ag (red peaks in Figure S17 centered at 374.2 and 368.2 eV) and Ag_2O (blue peaks centered at 373.6 and 367.6 eV).[12,34] The ratio of metallic Ag to oxidized Ag increases from 2.4 to 6 after one CO_2ER performance test, indicating the reduction of Ag_2O during this process.

In order to demonstrate the advantage of the LBL method over drop-casting, a carbon fiber (CF) supported Ag-CP electrode was prepared via the LBL method and the widely used drop-casting (DC) method (Scheme S1). When drop-casted, the Ag-CP particles spread around the carbon fibers, filling the space between them (Figure S18a,b). After electro-decomposition, large flower-like Ag particles grow onto the fibers, leaving a large part of the carbon support uncoated (Figure S18c,d). By comparison, the LBL method with 9 cycles produced uniformly dispersed Ag-CP (Figure S18e,f) and Ag particles (Figure S18g,h) fully covering the surface of carbon fibers.

Chronoamperometric (i.e., controlled-potential) electrochemical CO_2 reduction tests were carried out in a traditional two-compartment aqueous cell in a 0.1 M $KHCO_3$ electrolyte using a Pt counter electrode. The CO_2 electroreduction performance of Ag/MPL-*n*C electrodes is presented in Figure 4. Only CO and H_2 were detected as products by gas and liquid chromatography (GC and UPLC), and all the catalysts show stable CO_2ER performance after an initial 15 min period, where the in situ formation of the Ag/MPL takes place via electro-decomposition (Figure S19).

As shown in Figure 4a, the total geometrical current density increases with increasing cathode potential ($j_{Total,max}$ ≈ 43−44 mA cm^{-2} at around −1.05 V vs RHE for Ag/MPL-3,6C) along with the steady increase in the FE_{CO} (Figure 4b), reaching a maximum FE_{CO} of 90−95% (FE_{H_2} = 10−5%) between −0.6 and −1.1 V vs RHE for the Ag/MPL-1,2,3C electrodes. The number of LBL cycles also plays an important role in electrode performance, with 3 cycles showing the optimal compromise between the wide potential window for high FE_{CO} and the high j_{CO} (∼30 mA cm^{-2} at −1.0 V vs RHE) at a minimum Ag loading (Figure 4c and Table S6).

In order to investigate if the presence of linker molecules and Ag in the electrolyte solution affects CO_2ER performance, electrolysis was carried out at −2.0 and −1.6 V vs SCE using fresh electrolyte right after the in situ formation of the Ag/MPL-3C catalyst from the Ag-CP/MPL-3C precursor (Figure

DOI: 10.1021/acsenergylett.9b01509
ACS Energy Lett. 2019, 4, 2024−2031

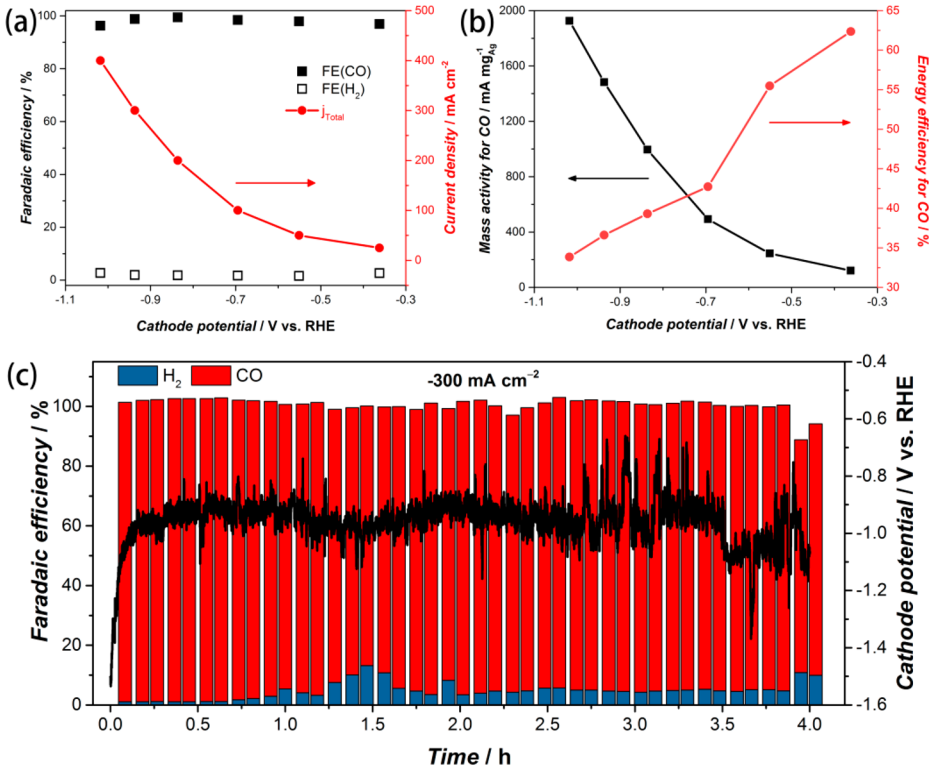

Figure 5. CO_2ER performance of the Ag/MPL-3C electrode in a gas-fed zero gap flow electrolyzer. (a) Faradaic efficiency and total current density and (b) mass activity energy efficiency for CO. (c) Stability test at −300 mA cm^{-2} for 4 h. The bar diagram represents the FE (left *y*-axis) of CO (red) and H_2 (blue), and the black line represents the cathode potential (right *y*-axis).

S20). No significant change in the product distribution was seen; however, the total current density drops by 15−25% after the change of the solution. We speculate that this is due to the loss of Ag from the surface rinsing the electrode. The long-term stability of the CO_2ER performance was also tested using the Ag/MPL-3C sample in a refreshed electrolyte solution, and stable CO_2-to-CO activity was attained in a 5 h electrolysis (Figure S21). The CO_2ER performance of the Ag/MPL-3C electrode was compared to similar Ag catalysts reported in the literature (Table S7).[12,14−19,35]

In order to address the increased j_{Total} and j_{CO}, the electrochemical active surface area (EASA) of the Ag-CP and Ag/MPL-*n*C samples was determined by the monolayer silver oxide method in 0.1 M KOH.[35,36] The charge for monolayer oxide formation was calculated in Figure S22. EASA almost linearly increases with ongoing LBL cycles (Figure S23), which then was not accompanied by the same increase in the total and CO current density. The latter levels off at 3 deposition cycles (Figure 4d). Even though the total amount of silver in Ag/MPL-6C increased considerably compared to Ag/MPL-3C (twice as many LBL cycles), it is not accompanied by the increase in the number of accessible active sites. The effect of electro-decomposition, i.e., the formation of Ag particles, can be followed in Figure S23. The EASA saturates after 2 LBL cycles at a lower level, as the increase in Ag loading (in the form of Ag-CP) is not followed by an increase of the number of active sites, demonstrating that only Ag in the outer surface acts as a CO_2-to-CO electrocatalyst.

CO_2 mass transport limitations are the bottleneck that prevent achieving high current densities in aqueous phase CO_2 electrolysis.[37,38] Therefore, we turned to a gas-fed flow electrolyzer to perform high current density chronopotentiometric CO_2 electrolysis on the Ag/MPL-3C electrode.[39−45] The cathode side was fed by a humidified CO_2 stream without using any liquid catholyte, and a nickel mesh was used as an oxygen evolution catalyst in recirculated 1 M KOH anolyte at the anode side. The two compartments were separated by Sustainion S-50 polyimidazolium-based anion exchange membrane. The catalytically active Ag particles were in situ formed from the presynthesized Ag-CP via an initial chronoamperometric run at constant −2 V vs Hg/HgO potential under CO_2 electroreduction conditions (Figure S24). CO was formed with high selectivity right from the beginning of the activation step, and j_{CO} levels off after about 20 min at typically around 200−300 mA cm^{-2}.

Immediately after the initial CA run, chronopotentiometric CO_2 electrolysis was done at different current densities. A moderately high current density of −25 mA cm^{-2} was achieved at a cathode potential of around −0.36 V vs RHE (Figure 5a). Toward higher current densities the cathode potential climbed to −1.04 V vs RHE, which corresponds to a cell voltage of 3.78 V, at j_{Total} = −400 mA cm^{-2}. High FE_{CO} (>96%) was achieved in the whole tested current density range, peaking at FE_{CO} = 99.5% at j_{Total} = −200 mA cm^{-2} ($E_{Cathode}$ = −0.84 V vs RHE). The flow cell CO_2ER performance of the Ag/MPL-3C catalyst is summarized in Table S8 and compared to literature data on high current density flow cell CO_2-to-CO electrolysis (Table S9 and Figure S25a).[16,46−58]

Active phase dispersion and accessibility plays a crucial role in catalytic performance. To this end, the MOF-mediated synthesis, combined with electro-decomposition, offers a straightforward approach to achieving high mass activity of the catalyst. In Ag/MPL-3C, the Ag-CP and Ag loading are 0.55 and 0.20−0.21 mg cm^{-2}, respectively, which in turn result

DOI: 10.1021/acsenergylett.9b01509
ACS Energy Lett. 2019, 4, 2024−2031

in a mass activity of 1864−1926 mA mg_{Ag}^{-1} (Figure 5b), one of the highest values ever reported (Table S9 and Figure S25b).[16,46−58] The energy efficiency of CO formation remains above 50% at moderate current densities (<100 mA cm^{-2}) and drops to the 32−42% range during high current density operation because of the elevated cell potential (Figure 5b). The main source of the low energy efficiencies is either the high overvoltage (energy wasted as dissipated heat) and/or low CO selectivity (energy wasted as undesired products).[37]

Ag/MPL-3C showed stable high current density performance at −300 mA cm^{-2} for 4 h (Figure 5c). The estimated average potential was −0.94 V vs RHE in the first 3.5 h. The fluctuation in the potential reading is due to the intensive bubble formation at the nickel mesh anode catalyst, as the counter electrode potential was directly determined in this setup. The cell potential oscillated at around 3.2 V in the first 3 h, then it shifted to higher voltages (Figure S26). Moreover, gas flow fluctuation due to carbonate precipitation in the cathode flow channels is a further issue to be solved in industrial scale high-rate operations in alkaline environment CO_2 electrolysis.[37,50] Images of a crystalline precipitate are seen after a long-term electrolysis in Figure S27 without (a) and with (b) reactant stream humidification; its XRD pattern (Figure S28) shows that mainly $KHCO_3$ was formed in the flow channels and on the macroporous side of the carbon cloth GDE. The temporary increase in FE_{H_2} at around 1.5 h is most probably the result of the building-up of the $KHCO_3$ layer on the cathode side of the cell. This on one hand partly blocks the CO_2 flow, but on the other hand, it provides a suitable environment for CO_2ER as the HCO_3^- ion layer at the cathode is known for stabilizing the CO_2ER performance in flow electrolyzers.[37,50]

In summary, the MOF-mediated approach, i.e., LBL deposition of Ag-CP followed by electro-decomposition, offers a facile route for manufacturing uniformly dispersed Ag catalysts for CO_2ER. In spite of the small amount of Ag in the final electrodes (0.2 mg cm^{-2}), gas diffusion electrodes show excellent CO_2ER performance in traditional aqueous cells ($FE_{CO} \approx 90-95\%$ and $j_{CO,max}$ = 38.8 mA cm^{-2} at −1.07 V vs RHE) and in a gas-fed electrolyzer ($j_{CO,max}$ = 385 mA cm^{-2} at −1.04 V vs RHE). The enhanced catalyst dispersion and utilization resulted in one of the highest silver mass activities (1864 mA mg_{Ag}^{-1}) in the literature to date. The direct synthesis of metal electrocatalyst eliminates the need for ill-defined deposition steps (drop-casting, etc.) while allowing tight control of the catalyst structure through self-assembly.

■ ASSOCIATED CONTENT

Supporting Information

The Supporting Information is available free of charge on the ACS Publications website at DOI: 10.1021/acsenergylett.9b01509.

Optimization of the synthetic conditions; crystal structure details; experimental details; figures of material characterization, including SEM, XRD, and XPS results; additional CO_2 electroreduction performance (PDF)

■ AUTHOR INFORMATION

Corresponding Author

*E-mail: jorge.gascon@kaust.edu.sa.

ORCID

Samy Ould-Chikh: 0000-0002-3486-0944

Wilson A. Smith: 0000-0001-7757-5281

Freek Kapteijn: 0000-0003-0575-7953

Jorge Gascon: 0000-0001-7558-7123

Notes

The authors declare no competing financial interest.

■ ACKNOWLEDGMENTS

The authors thank China Scholarship Council (CSC) and TOTAL for financial support.

■ REFERENCES

(1) Kondratenko, E. V.; Mul, G.; Baltrusaitis, J.; Larrazabal, G. O.; Perez-Ramirez, J. Status and perspectives of CO_2 conversion into fuels and chemicals by catalytic, photocatalytic and electrocatalytic processes. *Energy Environ. Sci.* **2013**, *6* (11), 3112−3135.

(2) Saeidi, S.; Amin, N. A. S.; Rahimpour, M. R. Hydrogenation of CO_2 to value-added products-A review and potential future developments. *Journal of Co2 Utilization* **2014**, *5*, 66−81.

(3) Sharma, S.; Hu, Z. P.; Zhang, P.; McFarland, E. W.; Metiu, H. CO_2 methanation on Ru-doped ceria. *J. Catal.* **2011**, *278* (2), 297−309.

(4) Thampi, K. R.; Kiwi, J.; Gratzel, M. Methanation and Photo-Methanation of Carbon-Dioxide at Room-Temperature and Atmospheric-Pressure. *Nature* **1987**, *327* (6122), 506−508.

(5) Wang, W.; Wang, S.; Ma, X.; Gong, J. Recent advances in catalytic hydrogenation of carbon dioxide. *Chem. Soc. Rev.* **2011**, *40* (7), 3703−27.

(6) Whipple, D. T.; Kenis, P. J. A. Prospects of CO_2 Utilization via Direct Heterogeneous Electrochemical Reduction. *J. Phys. Chem. Lett.* **2010**, *1* (24), 3451−3458.

(7) Lu, Q.; Jiao, F. Electrochemical CO 2 reduction: Electrocatalyst, reaction mechanism, and process engineering. *Nano Energy* **2016**, *29*, 439−456.

(8) Ganesh, I. Electrochemical conversion of carbon dioxide into renewable fuel chemicals - The role of nanomaterials and the commercialization. *Renewable Sustainable Energy Rev.* **2016**, *59*, 1269−1297.

(9) Zhu, W.; Michalsky, R.; Metin, O.; Lv, H.; Guo, S.; Wright, C. J.; Sun, X.; Peterson, A. A.; Sun, S. Monodisperse Au nanoparticles for selective electrocatalytic reduction of CO_2 to CO. *J. Am. Chem. Soc.* **2013**, *135* (45), 16833−6.

(10) Mistry, H.; Reske, R.; Zeng, Z.; Zhao, Z. J.; Greeley, J.; Strasser, P.; Cuenya, B. R. Exceptional size-dependent activity enhancement in the electroreduction of CO_2 over Au nanoparticles. *J. Am. Chem. Soc.* **2014**, *136* (47), 16473−6.

(11) Sastre, F.; Munoz-Batista, M. J.; Kubacka, A.; Fernandez-Garcia, M.; Smith, W. A.; Kapteijn, F.; Makkee, M.; Gascon, J. Efficient Electrochemical Production of Syngas from CO_2 and H_2O by using a Nanostructured Ag/g-C3N4 Catalyst. *ChemElectroChem* **2016**, *3* (9), 1497−1502.

(12) Ma, M.; Trzesniewski, B. J.; Xie, J.; Smith, W. A. Selective and Efficient Reduction of Carbon Dioxide to Carbon Monoxide on Oxide-Derived Nanostructured Silver Electrocatalysts. *Angew. Chem., Int. Ed.* **2016**, *55* (33), 9748−52.

(13) Won, D. H.; Shin, H.; Koh, J.; Chung, J.; Lee, H. S.; Kim, H.; Woo, S. I. Highly Efficient, Selective, and Stable CO_2 Electroreduction on a Hexagonal Zn Catalyst. *Angew. Chem., Int. Ed.* **2016**, *55* (32), 9297−9300.

(14) Daiyan, R.; Lu, X. Y.; Ng, Y. H.; Amal, R. Highly Selective Conversion of CO_2 to CO Achieved by a Three-Dimensional Porous Silver Electrocatalyst. *Chemistryselect* **2017**, *2* (3), 879−884.

(15) Liu, S.; Tao, H.; Zeng, L.; Liu, Q.; Xu, Z.; Liu, Q.; Luo, J. L. Shape-Dependent Electrocatalytic Reduction of CO_2 to CO on Triangular Silver Nanoplates. *J. Am. Chem. Soc.* **2017**, *139* (6), 2160−2163.

DOI: 10.1021/acsenergylett.9b01509
ACS Energy Lett. 2019, 4, 2024−2031

(16) Lu, Q.; Rosen, J.; Zhou, Y.; Hutchings, G. S.; Kimmel, Y. C.; Chen, J. G.; Jiao, F. A selective and efficient electrocatalyst for carbon dioxide reduction. *Nat. Commun.* **2014**, *5*, 3242.
(17) Mistry, H.; Choi, Y. W.; Bagger, A.; Scholten, F.; Bonifacio, C. S.; Sinev, I.; Divins, N. J.; Zegkinoglou, I.; Jeon, H. S.; Kisslinger, K.; Stach, E. A.; Yang, J. C.; Rossmeisl, J.; Roldan Cuenya, B. Enhanced Carbon Dioxide Electroreduction to Carbon Monoxide over Defect-Rich Plasma-Activated Silver Catalysts. *Angew. Chem., Int. Ed.* **2017**, *56* (38), 11394−11398.
(18) Peng, X.; Karakalos, S. G.; Mustain, W. E. Preferentially Oriented Ag Nanocrystals with Extremely High Activity and Faradaic Efficiency for CO_2 Electrochemical Reduction to CO. *ACS Appl. Mater. Interfaces* **2018**, *10* (2), 1734−1742.
(19) Rosen, B. A.; Salehi-Khojin, A.; Thorson, M. R.; Zhu, W.; Whipple, D. T.; Kenis, P. J.; Masel, R. I. Ionic liquid-mediated selective conversion of CO(2) to CO at low overpotentials. *Science* **2011**, *334* (6056), 643−4.
(20) Hori, Y.; Kikuchi, K.; Suzuki, S. Production of CO and Ch4 in Electrochemical Reduction of CO_2 at Metal-Electrodes in Aqueous Hydrogencarbonate Solution. *Chem. Lett.* **1985**, *14*, 1695−1698.
(21) Wang, R.; Sun, X.; Ould-Chikh, S.; Osadchii, D.; Bai, F.; Kapteijn, F.; Gascon, J. Metal-Organic-Framework-Mediated Nitrogen-Doped Carbon for CO_2 Electrochemical Reduction. *ACS Appl. Mater. Interfaces* **2018**, *10* (17), 14751−14758.
(22) Jhong, H.-R. M.; Brushett, F. R.; Kenis, P. J. A. The Effects of Catalyst Layer Deposition Methodology on Electrode Performance. *Adv. Energy Mater.* **2013**, *3* (5), 589−599.
(23) Sun, X.; Suarez, A. I. O.; Meijerink, M.; van Deelen, T.; Ould-Chikh, S.; Zecevic, J.; de Jong, K. P.; Kapteijn, F.; Gascon, J. Manufacture of highly loaded silica-supported cobalt Fischer−Tropsch catalysts from a metal organic framework. *Nat. Commun.* **2017**, *8* (1), 1680.
(24) Sun, X.; Olivos-Suarez, A. I.; Osadchii, D.; Romero, M. J. V.; Kapteijn, F.; Gascon, J. Single cobalt sites in mesoporous N-doped carbon matrix for selective catalytic hydrogenation of nitroarenes. *J. Catal.* **2018**, *357*, 20−28.
(25) Sun, X.; Olivos-Suarez, A. I.; Oar-Arteta, L.; Rozhko, E.; Osadchii, D.; Bavykina, A.; Kapteijn, F.; Gascon, J. Metal-Organic Framework Mediated Cobalt/Nitrogen-Doped Carbon Hybrids as Efficient and Chemoselective Catalysts for the Hydrogenation of Nitroarenes. *ChemCatChem* **2017**, *9* (10), 1854−1862.
(26) Santos, V. P.; Wezendonk, T. A.; Jaen, J. J.; Dugulan, A. I.; Nasalevich, M. A.; Islam, H. U.; Chojecki, A.; Sartipi, S.; Sun, X.; Hakeem, A. A.; Koeken, A. C.; Ruitenbeek, M.; Davidian, T.; Meima, G. R.; Sankar, G.; Kapteijn, F.; Makkee, M.; Gascon, J. Metal organic framework-mediated synthesis of highly active and stable Fischer−Tropsch catalysts. *Nat. Commun.* **2015**, *6*, 6451.
(27) Oar-Arteta, L.; Wezendonk, T.; Sun, X. H.; Kapteijn, F.; Gascon, J. Metal organic frameworks as precursors for the manufacture of advanced catalytic materials. *Materials Chemistry Frontiers* **2017**, *1* (9), 1709−1745.
(28) Wang, R.; Kapteijn, F.; Gascon, J. Engineering Metal−Organic Frameworks for the Electrochemical Reduction of CO_2: A Minireview. *Chem. - Asian J.* **2019**. DOI: 10.1002/asia.201900710.
(29) Lu, X.; Ye, J.; Zhang, D.; Xie, R.; Bogale, R. F.; Sun, Y.; Zhao, L.; Zhao, Q.; Ning, G. Silver carboxylate metal-organic frameworks with highly antibacterial activity and biocompatibility. *J. Inorg. Biochem.* **2014**, *138*, 114−121.
(30) Pawley, G. S. Unit-Cell Refinement from Powder Diffraction Scans. *J. Appl. Crystallogr.* **1981**, *14* (Dec), 357−361.
(31) Boultif, A.; Louer, D. Powder pattern indexing with the dichotomy method. *J. Appl. Crystallogr.* **2004**, *37*, 724−731.
(32) Altomare, A.; Corriero, N.; Cuocci, C.; Falcicchio, A.; Moliterni, A.; Rizzi, R. EXPO software for solving crystal structures by powder diffraction data: methods and application. *Cryst. Res. Technol.* **2015**, *50* (9−10), 737−742.
(33) L'vov, B. V. Kinetics and mechanism of thermal decomposition of silver oxide. *Thermochim. Acta* **1999**, *333* (1), 13−19.
(34) Gao, X. Y.; Wang, S. Y.; Li, J.; Zheng, Y. X.; Zhang, R. J.; Zhou, P.; Yang, Y. M.; Chen, L. Y. Study of structure and optical properties of silver oxide films by ellipsometry, XRD and XPS methods. *Thin Solid Films* **2004**, *455*, 438−442.
(35) Ma, M.; Liu, K.; Shen, J.; Kas, R.; Smith, W. A. In Situ Fabrication and Reactivation of Highly Selective and Stable Ag Catalysts for Electrochemical CO_2 Conversion. *ACS Energy Letters* **2018**, *3* (6), 1301−1306.
(36) Rosen, J.; Hutchings, G. S.; Lu, Q.; Rivera, S.; Zhou, Y.; Vlachos, D. G.; Jiao, F. Mechanistic Insights into the Electrochemical Reduction of CO_2 to CO on Nanostructured Ag Surfaces. *ACS Catal.* **2015**, *5* (7), 4293−4299.
(37) Martín, A. J.; Larrazábal, G. O.; Pérez-Ramírez, J. Towards sustainable fuels and chemicals through the electrochemical reduction of CO_2: lessons from water electrolysis. *Green Chem.* **2015**, *17* (12), 5114−5130.
(38) Schwarz, H. A.; Dodson, R. W. Reduction potentials of CO_2- and the alcohol radicals. *J. Phys. Chem.* **1989**, *93* (1), 409−414.
(39) Han, L.; Zhou, W.; Xiang, C. High-Rate Electrochemical Reduction of Carbon Monoxide to Ethylene Using Cu-Nanoparticle-Based Gas Diffusion Electrodes. *ACS Energy Letters* **2018**, *3* (4), 855−860.
(40) Burdyny, T.; Smith, W. A. CO_2 reduction on gas-diffusion electrodes and why catalytic performance must be assessed at commercially-relevant conditions. *Energy Environ. Sci.* **2019**, *12*, 1442.
(41) Higgins, D.; Hahn, C.; Xiang, C.; Jaramillo, T. F.; Weber, A. Z. Gas-Diffusion Electrodes for Carbon Dioxide Reduction: A New Paradigm. *ACS Energy Letters* **2019**, *4* (1), 317−324.
(42) Wu, J.; Risalvato, F. G.; Sharma, P. P.; Pellechia, P. J.; Ke, F.-S.; Zhou, X.-D. Electrochemical Reduction of Carbon Dioxide. *J. Electrochem. Soc.* **2013**, *160* (9), F953−F957.
(43) Merino-Garcia, I.; Alvarez-Guerra, E.; Albo, J.; Irabien, A. Electrochemical membrane reactors for the utilisation of carbon dioxide. *Chem. Eng. J.* **2016**, *305*, 104−120.
(44) Endrődi, B.; Bencsik, G.; Darvas, F.; Jones, R.; Rajeshwar, K.; Janáky, C. Continuous-flow electroreduction of carbon dioxide. *Prog. Energy Combust. Sci.* **2017**, *62*, 133−154.
(45) Weekes, D. M.; Salvatore, D. A.; Reyes, A.; Huang, A.; Berlinguette, C. P. Electrolytic CO_2 Reduction in a Flow Cell. *Acc. Chem. Res.* **2018**, *51* (4), 910−918.
(46) Ma, S.; Luo, R.; Gold, J. I.; Yu, A. Z.; Kim, B.; Kenis, P. J. A. Carbon nanotube containing Ag catalyst layers for efficient and selective reduction of carbon dioxide. *J. Mater. Chem. A* **2016**, *4* (22), 8573−8578.
(47) Ma, S.; Luo, R.; Moniri, S.; Lan, Y.; Kenis, P. J. A. Efficient Electrochemical Flow System with Improved Anode for the Conversion of CO_2 to CO. *J. Electrochem. Soc.* **2014**, *161* (10), F1124−F1131.
(48) Ma , S.; Lan , Y.; Perez, G. M. J.; Moniri, S.; Kenis , P. J. A. Silver Supported on Titania as an Active Catalyst for Electrochemical Carbon Dioxide Reduction. *ChemSusChem* **2014**, *7* (3), 866−874.
(49) Tornow, C. E.; Thorson, M. R.; Ma, S.; Gewirth, A. A.; Kenis, P. J. A. Nitrogen-Based Catalysts for the Electrochemical Reduction of CO_2 to CO. *J. Am. Chem. Soc.* **2012**, *134* (48), 19520−19523.
(50) Verma, S.; Hamasaki, Y.; Kim, C.; Huang, W.; Lu, S.; Jhong, H.-R. M.; Gewirth, A. A.; Fujigaya, T.; Nakashima, N.; Kenis, P. J. A. Insights into the Low Overpotential Electroreduction of CO_2 to CO on a Supported Gold Catalyst in an Alkaline Flow Electrolyzer. *ACS Energy Letters* **2018**, *3* (1), 193−198.
(51) Verma, S.; Lu, X.; Ma, S.; Masel, R. I.; Kenis, P. J. A. The effect of electrolyte composition on the electroreduction of CO_2 to CO on Ag based gas diffusion electrodes. *Phys. Chem. Chem. Phys.* **2016**, *18* (10), 7075−7084.
(52) Dinh, C.-T.; García de Arquer, F. P.; Sinton, D.; Sargent, E. H. High Rate, Selective, and Stable Electroreduction of CO_2 to CO in Basic and Neutral Media. *ACS Energy Letters* **2018**, *3* (11), 2835−2840.

DOI: 10.1021/acsenergylett.9b01509
ACS Energy Lett. 2019, 4, 2024−2031

(53) Haas, T.; Krause, R.; Weber, R.; Demler, M.; Schmid, G. Technical photosynthesis involving CO_2 electrolysis and fermentation. *Nature Catalysis* **2018**, *1* (1), 32−39.
(54) Jhong, H.-R. M.; Tornow, C. E.; Kim, C.; Verma, S.; Oberst, J. L.; Anderson, P. S.; Gewirth, A. A.; Fujigaya, T.; Nakashima, N.; Kenis, P. J. A. Gold Nanoparticles on Polymer-Wrapped Carbon Nanotubes: An Efficient and Selective Catalyst for the Electroreduction of CO_2. *ChemPhysChem* **2017**, *18* (22), 3274−3279.
(55) Jhong, H.-R. M.; Tornow, C. E.; Smid, B.; Gewirth, A. A.; Lyth, S. M.; Kenis, P. J. A. A Nitrogen-Doped Carbon Catalyst for Electrochemical CO_2 Conversion to CO with High Selectivity and Current Density. *ChemSusChem* **2017**, *10* (6), 1094−1099.
(56) Kim, B.; Hillman, F.; Ariyoshi, M.; Fujikawa, S.; Kenis, P. J. A. Effects of composition of the micro porous layer and the substrate on performance in the electrochemical reduction of CO_2 to CO. *J. Power Sources* **2016**, *312*, 192−198.
(57) Ma, S.; Liu, J.; Sasaki, K.; Lyth, S. M.; Kenis, P. J. A. Carbon Foam Decorated with Silver Nanoparticles for Electrochemical CO_2 Conversion. *Energy Technology* **2017**, *5* (6), 861−863.
(58) Möller, T.; Ju, W.; Bagger, A.; Wang, X.; Luo, F.; Ngo Thanh, T.; Varela, A. S.; Rossmeisl, J.; Strasser, P. Efficient CO_2 to CO electrolysis on solid Ni−N−C catalysts at industrial current densities. *Energy Environ. Sci.* **2019**, *12* (2), 640−647.

DOI: 10.1021/acsenergylett.9b01509
ACS Energy Lett. 2019, 4, 2024−2031